nature communications

Article

https://doi.org/10.1038/s41467-026-77804-6

Independent assembly of the flight apparatus in a non-avian dinosaur clade

Received: 22 January 2026

Accepted: 4 September 2026

Published online: 29 September 2026

Check for updates

Xuri Wang[1,2], Yannan Ji[3], Andrea Cau[4] ✉, Martin Kundrát[5], Yichuan Liu[1,6], Yang Wang[1] & Qiang Ji[2] ✉

The discovery of feathered dinosaurs revolutionized the studies on the origin of birds and the evolution of their flight. Among paravians (birds and their closest relatives), the microraptorine dromaeosaurids are unique in bearing several flight-related adaptations with a controversial evolutionary interpretation, supporting, alternatively, flight as ancestral to Paraves or having evolved multiple times among the latter. Here, we introduce an exquisitely-preserved member of Microraptorinae, *Norellraptor barsboldi* gen. et sp. nov., and describe in detail forelimb osteohistological features for that clade. *Norellraptor* nests among late-diverging microraptorines and supports step-wise assembly of aerial adaptations in that clade. About 30% of the microraptorine synapomorphies are convergently acquired by the bird lineage (Avialae). Yet, the sequences of flight-related novelties reconstructed along the two lineages differ consistently; combined with histological evidence which might indicate a peculiar limb growth model in Microraptorinae, these results dismiss a shared developmental pattern driving the evolution of the flying dinosaurs and support multiple and independent selective regimes at the origin of the winged taxa in Paraves.

Microraptorinae is a clade of small-sized theropod dinosaurs mainly known from the Lower Cretaceous Jehol Biota of north-eastern China[1–10]. Feather-like integumentary structures, true pennaceous feathers and remnants of the gut contents are found in exceptionally-preserved microraptorines, providing details of their anatomy and ecology rarely available for dinosaur fossils[4,8,11–15]. As members of Paraves, microraptorines are among the closest relatives of birds[5,7,10,11] and display a peculiar combination of features in the limb and plumage which suggests that at least some members of the clade had acquired aerial adaptations[4,10,16–19]. Accordingly, microraptorines have been advocated as models for investigating the origin and evolution of the avian flight[4,10]. Yet, the evolutionary relationships between the flight apparatus of birds and the purported aerial adaptations of the microraptorines are controversial from both functional and phylogenetic perspectives[10]. Microraptorines are usually interpreted as early-diverging dromaeosaurids and sister taxon of Eudromaeosauria[7,10,20], a clade of mid-sized ground-dwelling theropods lacking the flight adaptations reported in microraptorines[7,10,21,22]. The similarities between microraptorines and birds have been interpreted as convergences due to analogous functional adaptations, a scenario implying at least two independent origins of flight among Paraves[10]. Alternatively, an incipient form of flight arose at the root of the paravian clade, being then inherited (and elaborated) among birds and microraptorines and secondarily lost by other paravians (e.g., eudromaeosaurs), a scenario involving an "incomplete synapomorphy"[23] which might explain the potential for powered flight widespread in several branches of Paraves[10].

Although usually meant as the direct expression of ancestry (i.e., a synapomorphy inherited from the last common ancestor), biological similarity between closely related taxa could also be the indirect result

[1]Key Laboratory of Stratigraphy and Paleontology of the Ministry of Natural Resources, Institute of Geology, Chinese Academy of Geological Sciences, Beijing, China. [2]Hebei GEO University, Shijiazhuang, Hebei Province, China. [3]Chinese Academy of Geological Sciences, Beijing, China. [4]OPHIS Museo Paleontologico e Centro Erpetologico, Teramo I-64100, Italy. [5]Center for Interdisciplinary Biosciences, Technology and Innovation Park, University of Pavol Jozef Šafárik, Košice, Slovakia. [6]China University of Geosciences, Beijing, China. ✉e-mail: cauand@gmail.com; jiqiang@hgu.edu.cn

of developmental constraints (i.e., a shared developmental pattern enforcing a preferred direction to the evolutionary change) which might result in the patchy distribution of the same derived condition among distinct members of a clade[23–27]. The recognition of a recurrent evolutionary pattern along distinct branches of one clade might inform on a shared (yet latent[23,25]) developmental homology synapomorphic for that clade (e.g., the evolutionary acquisition of the bird-like postcranial skeletal pneumatization among distinct branches of Saurischia or, alternatively, Ornithodira, might express a shared pattern driving the development of the air sacs along the avian total group[26]). Accordingly, if the recurrent evolution of aerial adaptations among the Mesozoic paravians is the expression of a shared developmental model among the members of that clade, it is expected that the assembly of the flight apparatus along the microraptorine and avialan lineages recapitulated a recurrent pattern.

Here, we describe a new exceptionally-preserved feathered dinosaur specimen from China and refer it to the new microraptorine *Norellraptor barsboldi* gen. et sp. nov. (Figs. 1–2). We compare the evolution of the flight-related adaptations among the microraptorine and avialan lineages and discuss the hypothesis that the two processes shared a pattern inherited from their common ancestry ("incomplete synapomorphy" *sensu*[23]).

Results

Systematic palaeontology

Dinosauria Owen, 1842 *sensu*[28]

Theropoda Marsh, 1881 *sensu*[28]

Dromaeosauridae Matthew and Brown, 1922 *sensu*[7]

Microraptorinae Senter et al., 2004[5]

Microraptorini (Senter et al., 2004)[5]

Norellraptor barsboldi gen. et sp. nov.

Holotype

130108-MHGU-F4281 (Figs. 1–3; Supplementary Table 1). The complete skeleton of a microraptorine dinosaur with part of the plumage imprints (Supplementary Fig. 1).

Locality and horizon

Lamadong Town, Jianchang County, western Liaoning, China. Jiufotang Formation, Lower Cretaceous. China.

Etymology

The genus name refers to the American palaeontologist Mark Allen Norell (1957-2025), with Latin word "*raptor*" ("robber"), a frequently used suffix in dromaeosaurid taxonomy. The species name refers to the Mongolian palaeontologist Rinchen Barsbold (1935-2025). The new taxon name remarks and honours the exceptional contributions by R. Barsbold and M. A. Norell to the study of the bird-like dinosaurs.

Diagnosis

Microraptorine dromaeosaurid with the unique combination of features (autapomorphies marked by asterisk; Supplementary Fig. 2): premaxilla with length of prenarial part half the depth of the subnarial body; large promaxillary fenestra occupying the whole rostral third of the antorbital fossa*, and with long axis inclined 35° caudodorsally; *pila promaxillaris* narrower than the *pila interfenestralis* and both less than half the diameter of the maxillary fenestra*; pubis gently curved caudoventrally with small foot having the posterior projection less than the diameter of the pubic shaft*. Differential diagnosis: *Norellraptor* differs from *Changyuraptor* in having basally-constricted dentary crowns and in the semilunate carpal barely capping the second metacarpal; from *Graciliraptor* in having the distal end of metatarsal II subequal in width to metatarsal III; from *Microraptor* in having the rostralmost maxillary teeth proportionally larger and the first three dentary teeth not procumbent, in the presence of a bulbous distal

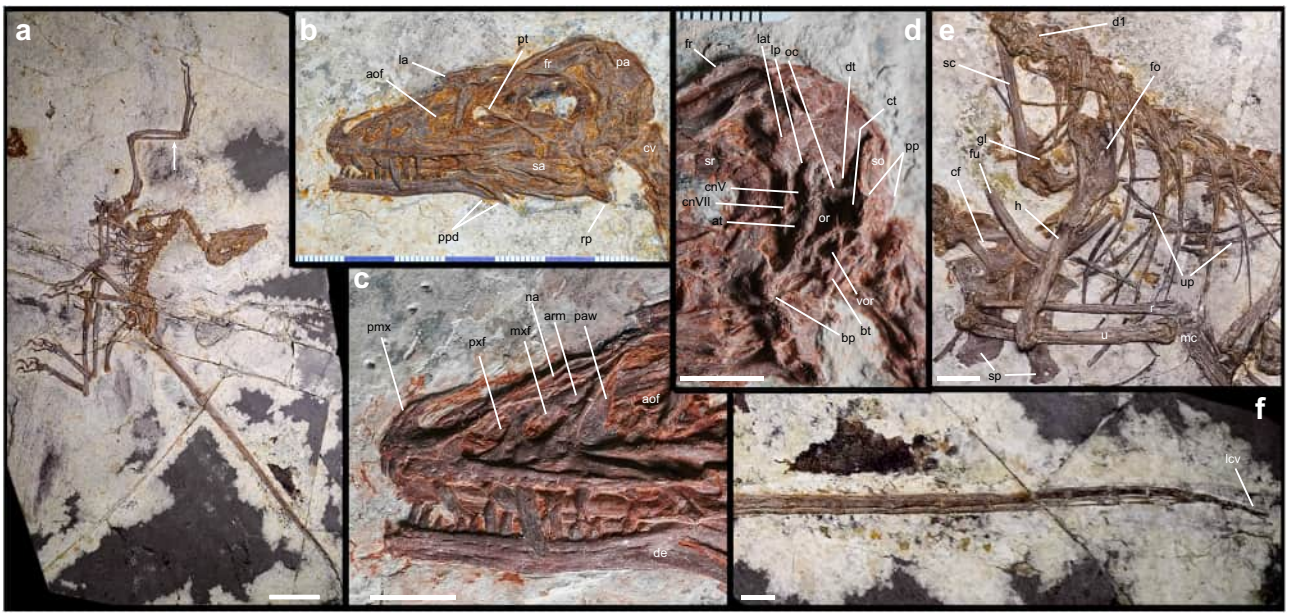

Fig. 1 | *Norellraptor barsboldi* 130108-MHGU-F4281. a Whole specimen. **b** Skull in lateral view. **c** Close up of the rostrum. **d** Close up of the posterior part of skull. **e** Pectoral region. **f** Distal end of tail. aof, antorbital fossa; arm, ascending ramus of maxilla; at, anterior tympanic recess; bt, basal tuber; bp, basypterygoid process; cf, coracoid fenestra; ct, caudal tympanic recess; cnV, 5th cranial nerve opening; cnVII, 7th cranial nerve opening; cv, cervical vertebra; d1, first dorsal vertebra; de, dentary; dt, dorsal tympanic recess; fo, foramen; fr, frontal; fu, furcula; gl, glenoid; h, humerus; la, lacrimal; lat, laterosphenoid; lcv, last caudal vertebra; lp, lateral pneumatic recess; mc, metacarpus; mxf, maxillary fenestra; na, nasal; oc, otosphenoid crest; or, otic region; pa, parietal; paw, postantral wall; pmx, premaxilla; pp, paroccipital process; ppd, posterior processes of dentary; pt, pterygoid; pxf, promaxillary fenestra; r, radius; rp, retroarticular process; sa, surangular; sc, scapula; so, supraoccipital; sp, sternal plate; sr, sclerotic ring; u, ulna; up, uncinate process; vor, ventral otic recess. Arrow indicates point of histological sampling. Scale bar = 50 mm (**a**); 10 mm (**b**–**f**).

https://doi.org/10.1038/s41467-026-77804-6

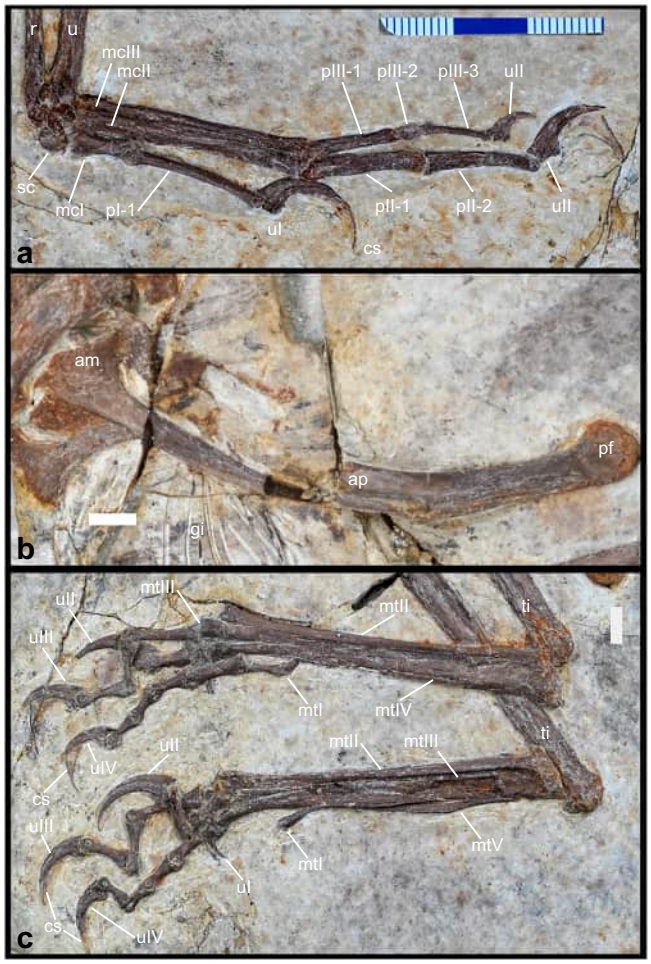

Fig. 2 | *Norellraptor barsboldi* 130108-MHGU-F4281, appendicular elements. **a** Right hand. **b** Pubis. **c** Feet. am, acetabular margin; ap, apron; cs, claw soft tissue; gi, gastral impression; mcI-III, metacarpals I to III; mtI-V, metatarsals I to V; p, phalanx; pf, pubic foot; r, radius; sc, semilunate carpal; t, tibiotarsus; u, ulna; uI-III, unguals 1 to 3. Scale bar = 10 mm.

process of the ulna, in having the arctometatarsalian tarsometatarsus, and in the more extensive fusion between the proximal shafts of metatarsals II to IV; from *Hesperonychus* and *Sinornithosaurus* in having a proportionally much smaller pubic foot; from *Wulong* in the relative size of the promaxillary and maxillary fenestrae in the antorbital fossa; and from *Zhongjianosaurus* in the proportionally shorter tail and sternum relative to the femur, in the more prominent lateral process of the coracoid, in the proportionally shorter and more gracile forelimb compared to the hindlimb, in the smaller deltopectoral fenestra, in the more moderate caudal inclination of the internal tuberosity of the humerus, in the semilunate carpal more convex proximally and covering most of the proximal surface of the first metacarpal, in the lack of a distinct ventral curvature of the penultimate manual phalanges, in the third manual ungual bearing a proximodorsal lip but being less curved ventrally, in the prominent proximolateral spur on the tarsometatarsus, and in the less elongate penultimate phalanx of the third toe.

Description and comparison

The 57 cm long skeleton is complete and suffered only a moderate disarticulation of the appendicular girdles (Fig. 1a). The histological analysis, complete fusion of the tibiotarsi and tarsometatarsi, and the smooth texture of the long bones support a post-juvenile developmental stage at the time of death[29].

The skull is subtriangular in lateral view, as in other microraptorines[9], with a vaulted frontoparietal region and a moderately elongated snout (Fig. 1b-d). The premaxilla is partially preserved and shows a prenarial body proportionally deeper and shorter than in *Microraptor* and *Sinornithosaurus*[9,30], with the rostral narial margin at the level of the distal end of the second alveolus. The premaxillary teeth are unserrated, as in most paravians. The maxilla is triradiate, similar to other microraptorines[9,29,30]. The rostral ramus is partially covered by the premaxilla. As in *Microraptor*[9], the caudodorsal ramus of the maxilla is very short, barely extending beyond the level of the ascending ramus. The jugal ramus is triangular, moderately elongate and shallower than the base of the rostral ramus. The depth of the subcutaneous part of the jugal ramus is lower than that of the caudal margin of the antorbital fossa: the two regions are separated by a distinct margin. The antorbital fenestra is "D"-shaped, 150% taller than long. The antorbital fossa is excavated by shallow pits, homologous to the more densely pitted surface in other microraptorines[30]. The caudal margin of the antorbital fossa is marked by a vertical ridge, which separates the fossa housing the maxillary fenestra from the antorbital fenestra. One diagnostic feature of *Norellraptor* is the significant fenestration of the maxillary antorbital fossa. The promaxillary fenestra is larger than the maxillary fenestra and occupies the whole rostral third of the antorbital fossa, differing from the much smaller fenestra in *Microraptor* and *Wulong*[9,29], and from the condition in *Sinornithosaurus*, whose premaxillary fenestra is larger than the maxillary fenestra but does not occupy the whole rostral third of the antorbital fossa[7,30]. The maxillary fenestra is enlarged. It is drop-shaped and placed equidistant from the antorbital and the promaxillary fenestrae: accordingly, the *pila interfenestralis* and *promaxillaris* are comparably narrow, with the latter narrower than the former and both not wider than half the diameter of the maxillary fenestra. This condition differs from *Microraptor* and *Wulong*, which show a much narrower *pila interfenestralis* and a broad *pila interpremaxillaris*, and from *Sinornithosaurus*, which shows both *pilae* proportionally broader[7,9,30]. As in *Microraptor*[9], the caudodorsal corner of the maxillary fenestra is not exposed in lateral view, being it roofed by a lip of bone oriented caudoventrally. This feature, absent in other dromaeosaurids[31], was originally considered unique of *Microraptor*, and is here reinterpreted as a synapomorphy of Microraptorini. The lacrimal is "T"-shaped, similar in proportion to other microraptorines[9]. The postorbital part of the dermal skull bar is eroded, revealing the braincase. The braincase bones are well-preserved and fused to each other (Fig. 1d), differing from the badly preserved condition in other microraptorines[9,29,30]. The lateral surface of the braincase is extensively pneumatized. An oval pit is present on the laterosphenoid, as in troodontids[32,33], and is confluent with the large trigeminal foramen. A sharp otosphenoidal crest separates the dorsal tympanic recess from the otic depression. The lateral surface of the prootic-basisphenoid, ventral to the otic depression, houses a large suboval recess, topographically homologous to the subotic recess of some troodontids[33], and which is placed more rostroventrally than the depressions alternatively termed "prootic" or "basipterygoid" recess in other dromaeosaurids (e.g., *Velociraptor*, *Tsaagan*[34,35]). The caudal tympanic recess is a large pit confluent with the posterodorsal margin of the otic depression. The paroccipital process of the exoccipital is stout and laterally directed, differing from the slender and pendant process in *Mahakala*[7]. The palatal elements are partially disarticulated and overlapped by other bones. The pterygoid is partially exposed inside the orbital cavity and crosses the disarticulated sclerotic ring. The dentary shows subparallel dorsal and ventral margins and is gently bowed ventrally at mid-length. The rostrodorsal corner of the dentary is beveled in lateral view, as in several dromaeosaurids. The caudal margin of the dentary is forked as in other microraptorines[7,9,29,30]. Only two premaxillary teeth are visible, and seven maxillary teeth are still inside their alveoli. At least 16 teeth are preserved in the left dentary, with possible two additional empty

https://doi.org/10.1038/s41467-026-77804-6

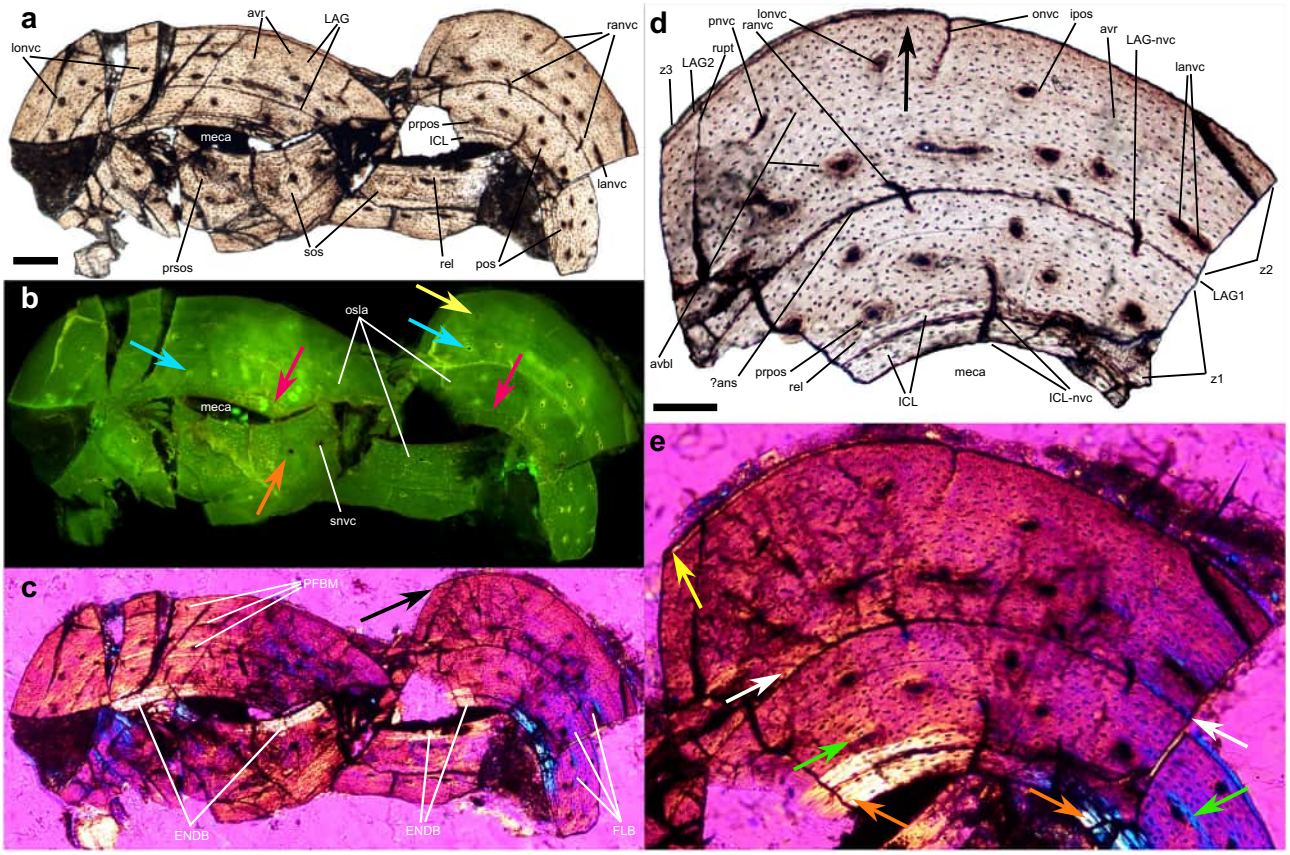

Fig. 3 | Histology of the left radius of 130108-MHGU-F4281. a–c close-up of the left radius midshaft microstructure (**d**, **e**). Physical transversal sections in transmitted (**a**, **d**), fluorescent (**b**), and elliptically polarized light (**c**, **e**). In **a**–**c**, note an irregular interface between the inner periosteal bone and the endosteal bone (red arrow); a high difference in fluorescence between well-developed primary osteons of the zone 1 and of the inner group of osteons of the zone 2 (blue arrow); and ill-developed primary of the outer group of osteons of the zone 2 (yellow arrow); a low fluorescene in the secondary osteonal bone (orange arrow). Compare the higher birefringence of the endosteal bone, an annulus-like tissue (white arrow), and early bone deposited to form zone 3 (black arrow). In **d**, **e**, note the occurence of more organized osteocyte lacunae in the outer region of zone 1 and througout the zone 2; increased birefringence in primary osteons of zone 1 (green arrow); in an annulus associate with LAG1 (white arrow) and zone 3 (yellow arrow); and highly birefringent endosteal bone tissue (orange arrow). Abbreviations:?ans, putative annulus; avbl, avascular layer; avr, avascular region; END, endosteal bone; FLB, fibro-lamellar bone; ICL, inner circumferential line; LAG, line of arrested growth; LAG-nvc, LAG crossing neurovascular canal; LAG1, inner circumferential layer; LAG2, outer line of arrested growth; ipos, ill developed primary osteon; lanvc, laminar neurovascular canal; lonvc, longitudinal neurovascular canal; meca, medullary cavity; onvc, neurovascular canal open on outer surface; osla, osteocyte lacuna; PER, periosteal bone; PFBM, parallel-fibered bone matrix; pos, primary osteon; pnvc, primary neurovascular canal; prpos, partially resorbed primary osteon; prsos, partially resorbed secondary osteon; ranvc, radial neurovascular canal; rel, resorption line; rupt, postfossilization rupture; snvc, secondary vascular canal; sos, secondary osteon; z1-3, first through third zone. Scale bar 200 microns (a-c) and 100 microns (**d**, **e**).

positions. The dentition is markedly anisodont, with the largest maxillary crown, placed ventral to the maxillary fenestra, being more than twice mesiodistally than the smallest erupted dentary crowns. The carinae of the best preserved teeth are serrated, bearing hooked denticles along the distal margin. The crowns of some dentary teeth are slightly basally constricted, similar to *Microraptor*[9].

The vertebral column is complete and articulated (Fig. 1a, e, f). The cervical series is hyperextended and exposed mainly in ventrolateral view. The dorsal vertebrae are exposed in lateral view and overlapped by the articulated ribs. The sacral series is covered by the pelvis. The number of caudal vertebrae is uncertain due to the extensive covering of the caudotheca which extends to the anteriormost caudal vertebrae as in other microraptorines[27]. The sternal plates are elongate, about 40% the length of the femur, with each plate about 160% as long as wide. The two sternal plates are not fused medially (Fig. 1e), differing from some *Microraptor* specimens[4]. The scapula is much shorter and gracile than the humerus, and is firmly fused to the coracoid. The latter is trapezoid, with a distinct proximal constriction between the scapular end and the main body. A large drop-shaped fenestra perforates the main body of the coracoid, as in other microraptorines (e.g., *Microraptor*, *Wulong*) and some eudromaeosaurs[36]. The sternal end of the coracoid bears a distinct lateral process. The humerus is shorter and less robust than the femur, differing from the more robust element in *Zhongjianosaurus*. The bone is sigmoid in lateral view, with the posteriorly bent proximal region followed by the straight shaft forming two-thirds of the bone (Fig. 1a, e). The proximal region bears a trapezoid deltopectoral crest which is perforated near its proximocranial margin by an elliptical fenestra, as in *Microraptor* but smaller than in *Zhongjianosaurus*[9,37]. Distally, the cranial surface of the humerus houses a distinct elliptical fossa placed immediately proximal to the distal articular condyles, as in other paravians[38]. A narrow distal notch separates the medial condyle from the entepicondyle. The radius is about 80% the length of the humerus, comparable to most microraptorines[4,9] but proportionally shorter than in *Zhongjianosaurus*. The distal end of the gently bowed ulna bears a bulbous process as in *Zhongjianosaurus*[37]. Both hands are complete and articulated with the forearms, forming with the latter an angle of about 100° (Fig. 2a). In the carpus, the large semilunate carpal caps the whole proximal end of the first metacarpal and abuts the medial half of the second metacarpal, similar to *Wulong*[29]. As in other microraptorines,

the first digit is proportionally shorter than in other non-avian theropods (i.e., the combined length of the first metacarpal and first phalanx is 0.87 of the second metacarpal, a value comparable to *Wulong* and many specimens of *Microraptor*[4,9,29]), the second finger is the most robust, and the third bears a diminutive second phalanx and an abbreviate penultimate phalanx shorter and more gracile then the first[4,9,29]. In the pelvis, the pubis is unique among microraptorines in the combination of moderately bowed shaft and reduced distal foot (Fig. 2b). The hindlimb is gracile-built and shows fully fused elements in both distal tibiotarsus and proximal tarsometatarsus, as in *Zhongjianosaurus* and mature specimens of *Microraptor*[37,39]. The medial condyle of the tibiotarsus is broadly rounded and extended proximally along its flexor side; the lateral condyle is more projected on the extensor direction. As in *Zhongjianosaurus*, the third metatarsal is strongly constricted proximally and overlapped by the adjacent metatarsals in its proximal fifth (Fig. 2c), an arctometatarsalian configuration absent in other dromaeosaurids[37,40]. As in other microraptorines but differing from *Zhongjianosaurus*, the tarsometatarsus bears a prominent proximolateral spur. As in other microraptorines[40], both ends of the second and third metatarsals are moderately ginglymoid, the fourth is the most robust, and the fifth is elongate and gently bowed laterally. The first toe is slender, with its ungual reaching the level of the second metatarso-phalangeal joint. The second toe is falciphoran as in most non-avialan paravians[41]. Both third and fourth toes bear a moderately elongate penultimate phalanx and curved unguals with robust flexor tubercles.

The plumage is preserved adjacent the right humerus and the synsacrum, ventral to the proximal caudal vertebrae, attached to the distal caudal vertebrae, ventral to the right tibiotarsus, and lateral to the right tarsometatarsus[1,4] (Supplementary Fig. 1). The exact length and detailed morphology of the plumage are difficult to be ascertained due to the bad preservation. The forelimb probably possesses asymmetrical pennaceous feathers, which are preserved medial to the right hand, but separated from the rest of the plumage. The feathers preserved in the distal end of the tail have a rachis-dominated morphology. The other preserved plumage is formed by straight, simple feathers, arranged tightly.

Osteohistology

We examined the forelimb histology based on successive physical transversal sections through the distal portion of the mid-diaphysis of the left radius (Fig. 3a-c). The mid-diaphysis collapsed and crushed post-mortem due to the pressure of accumulated overlaying sediment; however, its microstructure remained readable for high-resolution histological assessment within the sampled region (Fig. 3d-e).

The radius compacta is less than half a millimeter thick and varies from 365 μm to 487 μm. It surrounds a large medullary cavity (Fig. 3a). No evidence of trabecular structures is found within the medullary cavity, suggesting a high extension of pneumatization in the bone. The perimedullary region (= the inner periosteal region) is lined by lamellar bone tissue (Fig. 3b). This is the endosteal bone, labelled here also as the inner circumferential layer.

The endosteal bone (EB) is 38 μm to 65 μm thick and constitutes 8 to 15% of the compact bone thickness. The endosteal bone is highly birefringent (Fig. 3c); osteocyte lacunae are usually long and narrow (e.g., 12.9 μm x 2.7 μm – 6.8 μm x 3.3 μm). Occasionally, a vascular canal may project through the total profile of the bone (Fig. 3d).

The periosteal bone (PB) is 316 to 448 μm thick and constitutes 85 to 92% of the compact bone thickness; the PB/EB index varies from 5.8 to 11.7. The periosteal bone formation was interrupted twice. We classify these disruptions as LAGs (= lines of arrested growth). However, we have also identified a narrow rim of highly birefringent tissue with distinctly flattened lacunae that is deposited immediately centrifugally to the LAG1. This thin layer may represent an annulus-like resting mark (Fig. 3c; 3d). The two LAGs divide the periosteal bone into three zones, numbered in ascending order from inner to outer side (Fig. 3d).

Zone 1 is 81 μm to 180 μm thick. More than half of zone 1 has been resorbed, estimated based on the width of zone 2. The resorption proceeded at different rates along the perimedullar edge. Primary and secondary osteons are found truncated at the perimedullary region (Fig. 3a). Primary osteons are well-developed (Fig. 3b), and round to elliptical: for example, from 28.2 μm x 31.3 μm (with slightly oval neurovascular canal measuring, e.g., 8 μm x 10.7 μm) to 31.5 μm x 42.1 μm (with clearly oval neurovascular canal measuring, e.g., 10.1 μm x 14.4 μm). Primary neurovascular canals are distributed randomly, with density decreased at the outer margin of the zone. The canals are oriented longitudinally, except a few radial canals that are projected from the zone 1 into the zone 2 by crossing the LAG1 and the putative annulus (Fig. 3a). The compact bone is remodeled only within the zone 1, where secondary osteons of the first and second generation (e.g., 132.5 μm x 135.1 μm; with a diameter of the neurovascular canal: e.g., 28.9 × 33.7 μm) are found in a restricted region of the inner periosteal region. Osteocyte lacunae are randomly oriented in different directions and have an elongated shape; on our sections, they have oval to round outlines (e.g., 3.1 μm x 3.1 μm – 4.6 μm x 9.5 μm). The lacunae are distributed irregularly in the bone matrix, except those that participate in the formation of osteonal bone surrounding neurovascular canals.

Zone 2 is 205 μm to 255 μm thick. This is the only zone that was preserved entirely. It forms, in some directions, the outer edge of the radius compacta (Fig. 3d). Zone 2 consists exclusively of primary bone tissue. Neurovascular canals are arranged in two groups. The first (inner) group includes the canals (diameter: e.g., 7.9 μm x 15.1 μm; 9.8 μm x 16.3 μm) organized into one or two layers at the inner edge of zone 2. The canals are surrounded by well-developed osteons (diameter: e.g., 29.9 μm x 39.3 μm; 35.3 μm x 50.8 μm) and exhibit longitudinal, laminar, and radial projections. The inner group is separated from the outer (second) group of a few neurovascular canals (diameter: e.g., 8.7 μm x 12 μm). These canals are sporadic, smaller, and have an ill-developed osteonal bone (diameter: e.g., 27.5 μm x 35.6 μm). They project mainly longitudinally. Exceptionally, a neurovascular canal projecting radially can be seen to open on the outer surface of the bone (Fig. 3d). The inner and outer vasculature of zone 2 is separated by bone matrix, which shows a higher degree of organization of osteocytic lacunae; a similar situation can be observed immediately at the outer edge of zone 2. The osteocytic lacunae mostly maintain an almost round shape in cross section (e.g., 3.1 μm x 3.1 μm; 3.3 μm x 5.5 μm; 4.2 μm x 5.2 μm; to a lesser extent 4.6 μm x 9.5 μm). There is an increasing amount of parallel-fibered matrix component across zone 2, including the fibro-lamellar bone associated with the inner group of primary osteons.

Zone 3 is not a continuous layer of bone tissue with the thickest part measuring only 15.7 μm (Fig. 3d). Periosteal bone of zone 3 is highly birefringent (Fig. 3e), lacks vascularization, and osteocyte lacunae, which it contains, have an elongated shape (e.g., 5 μm x 20.6 μm to 9 μm x 25.6 μm).

Osteochronology and growth

The age assessment of the type specimen of *Norellraptor barsboldi* gen. et sp. nov. (130108-MHGU-F4281) was determined by the analysis of the radius compacta (Fig. 2a; 3a). Two distinct LAGs and incipient deposition of zone 3 indicate that the specimen lived for at least two years since hatching. However, relatively thin compacta compared with a large medullary cavity suggest a more cautious estimate, as it is reasonable to claim that besides substantial resorption of the zone 1 (earliest zone preserved), at least another zone was completely removed as well. Therefore, we suggest that 130108-MHGU-F4281 was minimally three years old when it died at the very beginning of the latest year of life. This value is intermediate between the ages inferred for the immature *Wulong bohaiensis*

holotype and *Sinornithosaurus*sp. DNHM-2140 (both less than 2 years old)[29] and that for the adult holotype of *Changyuraptor yangi* (at least five years old)[5].

Our assessment has taken several growth characteristics into account. The earliest recorded ontogeny already exhibits a decrease in vascularity towards the end of zone 1. The random pattern in the distribution of the neurovascular canal was not restored in zone 2. Although the unusual presence of radial neurovascular canals crossing the LAG1, we assume that relatively rapid growth was likely maintained during an early phase of the next season (represented here as zone 2). This is congruent with the deposition of fibrolamellar bone tissue associated, however, with a neurovascular canal arranged into a circumferential layer. Since the earliest stage of zone 2, a gradual increase is also observed in the distribution of osteocyte lacunae. Moreover, this phenomenon is accompanied by the occurrence of a birefringent component representing a parallel-fibered bone matrix. A radical change follows after this stage in the form of a thick deposition of avascular tissue. Vascularity was reduced abruptly and restricted to longitudinal projection. The latest deposited bone tissue of zone 2 remained avascular, except for a single radial neurovascular canal that opens externally. Osteocyte lacunae are organized more in rows, where the zone forms the outer surface of the radius. Remarkably, such an organization is not so obvious where an incipient bone of zone 3 is deposited. The well-developed and preserved zone 2 is followed by the earliest bone deposition recognized as zone 3 (Fig. 3), suggesting that the specimen died soon after the resumed bone formation. This suggests that zone 2 is characterized by changes in spatial organization of osteocyte lacunae that indicate variation in growth rates: randomly organized (higher rates) *versus* organized laminarly (growth slowing down). When the time profile of zone 2 is reconstructed, early bone was deposited at slower rates, followed by higher rates, and reversed to slower rates again towards the end. The earliest deposition of zone 3 does not exhibit the same distribution pattern of osteocyte lacunae (i.e., compare the laminar pattern occurring after LAG-1 *versus* the random one after LAG-2).

This unusual mixture of rapid-growth versus slow-growth characteristics may not only refer to reaching adulthood, but was perhaps related to (unknown) physiological troubles of the specimen. We conclude that 130108-MHGU-F4281 died early after the latest cessation of growth during the late juvenile period; the zone 3 bone deposit never became circumferentially complete. Bone formation prevailed over bone resorption. No signs of the external fundamental system are present.

The radial (forelimb) pattern in growth histology of 130108-MHGU-F4281 distinctly differs from the femoral (hindlimb) pattern in growth histology of the late juvenile *Microraptor* sp. DNHM-2842. The bone compacta is almost equally thick and includes a well-developed inner circumferential layer[15]. Contrary to the radius, the growth of the femur was not interrupted, and exhibits rather a gradual decrease in the number of still randomly distributed neurovascular canals. On the other hand, the radial pattern in juvenile growth histology of the microraptorine *Sinornithosaurus*sp. (DNHM-2140)[29] resembles that of *Norellraptor* (130108-MHGU-F4281), even though the late phase of zone 2 is missing in the former. It is noteworthy that in the juvenile specimens of *Sinornithosaurus* and *Wulong*, sampled fore- and hindlimb sections showed more similar histological patterns[29]. Furthermore, the radial pattern in growth histology of 130108-MHGU-F4281 is similar to the adult basal paravian *Aurornis xui* (YFGP-T5198[42]), with the exception that the second season is followed by the formation of the external fundamental system, and no radial neurovascular canals reach the outer surface of the bone. It remains to be tested if some basal dromaeosaurid and non-dromaeosaurid paravians evolved similar forearm growth osteohistology convergently, differing just in the timing of maturity.

Phylogenetic and macroevolutionary implications

Norellraptor is unique among dromaeosaurids in the extensive fenestration of the rostral part of the antorbital fossa due to the hypertrophy of both promaxillary and maxillary fenestrae separated by a narrow bar[9,29–31], and in the gently curved pubis ending in a small foot which differs from the more abruptly bent pubis bearing a prominent foot seen in other microraptorines[1,4,6,43]. Several derived features support the referral of *Norellraptor* to Microraptorinae and its sister taxon relationship with *Zhongjianosaurus* among the late-diverging members of that clade[4,9,37] (Fig. 4). In particular, the new microraptorine shares with *Zhongjianosaurus* a bulbous distal process of the ulna, the extensive fusion of the proximal metatarsal shafts, and the presence of the arctometatarsalian metatarsus (differing from the subarctometatarsalian condition in *Microraptor* and *Sinornithosaurus*[9,37,40]).

Under the phylogenetic framework reconstructed by our analyses, 194 apomorphies are optimized along the microraptorine internodes and terminal branches. About 30% of them (N = 57) are convergently acquired along the avialan internodes (Fig. 5). These features include the reduction of the nasal rami of the maxilla and lacrimal[9], the transition point placed proximal to the sixth caudal vertebra[9], the increased number of uncinate processes and the fusion of some processes to the ribs[37]; the increased number of sternal ribs[37]; the relatively elongate sternum and the midline fusion of the two blades[4,37], the presence of a prominent lateral process of the coracoid, the forelimb bones relatively robust compared to the hindlimb elements[37], the presence of a fenestra in the deltopectoral crest[9,37], the radial shaft significantly more gracile than the ulnar shaft[9], the ulna longer than the humerus[37], the fusion of the semilunate carpal with the metacarpus[37], the relatively short alular finger[4,9], the robust first phalanx of the second finger[9], the relatively shortened penultimate phalanx of the third finger[4,9], the caudally bowed pubis[3,9], the reduction of the pubic foot, the development of a prominent proximodorsal process on the ischium[3,4], the fusion of the proximal shafts of metatarsals II to IV[37], the relative elongation of the penultimate phalanx of the toes[9,37], the distal placement of the hallucal ungual[3]; the presence of ventrally curved and falciform toe unguals[9], and the presence of alular feathers[4]. Enforcing the microraptorines as members of Avialae, the shortest trees supporting that constraint are 23 steps longer than the shortest unenforced topologies: yet, even under those topologies, Microraptorinae resulted stem-ward to the long-tailed birds *Archaeopteryx* and anchiornithines. The hypothesis that the flight apparatus of microraptorines is synapomorphic with that of birds is thus strongly challenged from a quantitative perspective[5,7,10]. Furthermore, despite several flight-related adaptations shared by Avialae and Microraptorine, the evolutionary sequences reconstructing the acquisition of those features among the two clades did not follow a common pattern, and thus could not be considered the expression of a shared developmental regime[23–25]. For example, in Microraptorinae, a first set of transformations involved the relative shortening of the manual phalanges. These novelties include the first phalanx of pollex not extended distal to metacarpal II, and both penultimate phalanges in second and third fingers being shorter than the corresponding proximal phalanx: such features might be related to a reduction of the primitive grasping function in the hand[4,10,18,19] and occurred at the root of the clade. A second set of transformations include the fusion of the carpometacarpal elements, the opening of a fenestra in the deltopectoral crest and the relative elongation of the sternum, which instead are synapomorphic for the less inclusive subclade Microraptorini, and thus occurred later during the history of the group. In Avialae, on the contrary, the latter series of transformations occurred before those producing the shortening of the manual phalanges (respectively, at the roots of Pygostilia and Ornithothoraces). In conclusion, the distinct evolutionary histories of Microraptorinae and Avialae not only dismiss the common origin of their flight apparatuses,

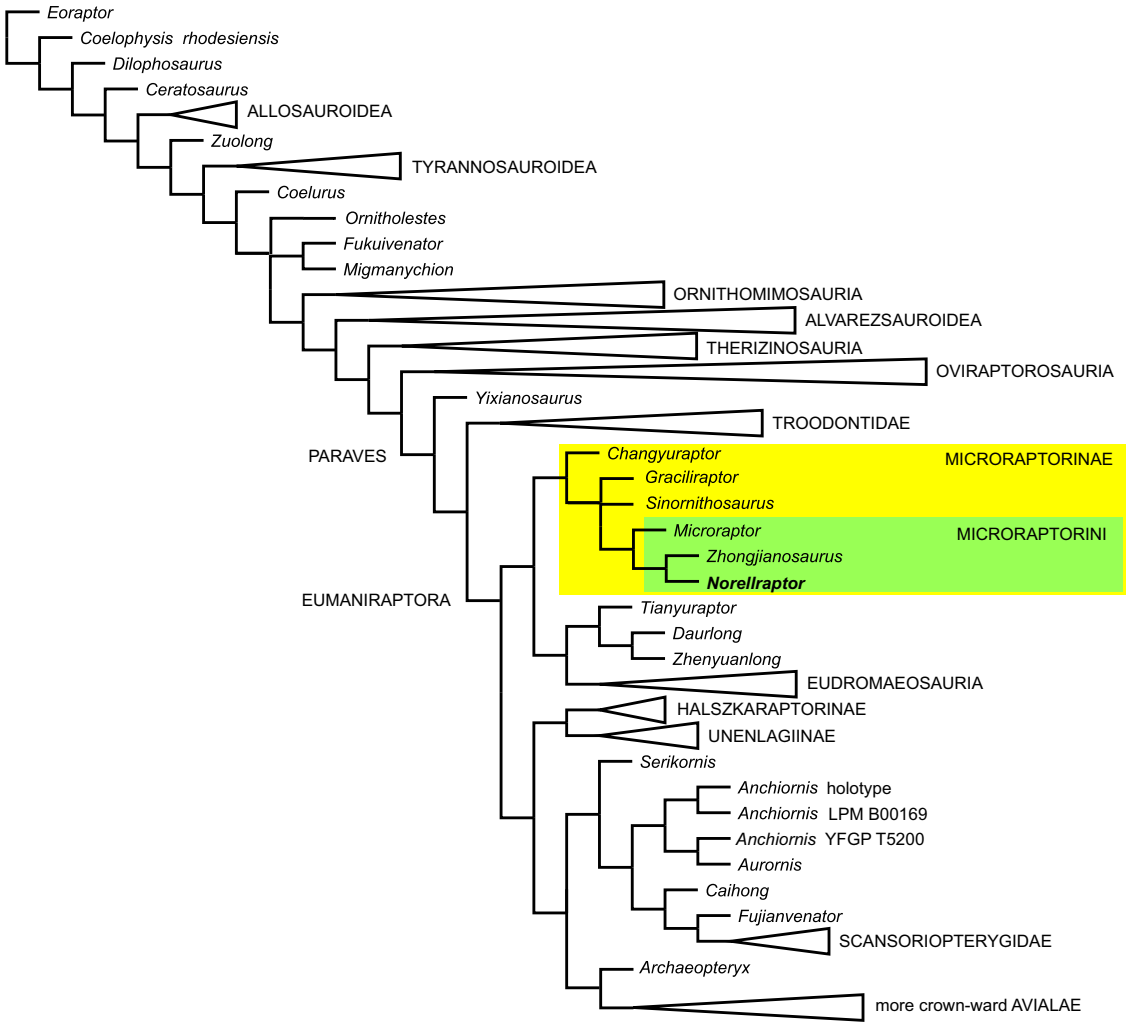

Fig. 4 | Simplified diagram of the phylogenetic relationships among Paraves. Collapsed clades indicated by the triangles (triangle areas proportional to the sampled taxa included: the complete topology reconstructed is available at https://doi.org/10.6084/m9.figshare.33006146.

but also challenge the hypothesis that a shared developmental regime acted as a single "deep homology" igniting the multiple and variegate evolution of aerial locomotion in Paraves.

The most significant result of our phylogenetic analysis is the placement of Halszkaraptorinae and Unenlagiinae closer to birds than dromaeosaurids and troodontids[44]. Although the paravian interrelationships suggested here challenge several studies supporting a morphologically more disparate Dromaeosauridae[7,20,27,31,36,38,41], our result independently replicates an alternative scenario which has focused on the numerous avian-like features present in the unenlagiids and not shared by the dromaeosaurids[44–47]. The re-evaluation of paravians like *Unenlagia* and *Halszkaraptor* as potentially closer proxies of the ancestral body plan of birds further calls into question the direct significance of the microraptorine aerial adaptations in reconstructing the origins of the avian flight[46].

Albeit preliminary, histological evidence from the Microraptorinae may further challenge the hypothesis that a common developmental regime shared with birds drove their aerial adaptations. In avian taxa with a growth pattern closer to the inferred non-avian theropod regime (precociality)[42] and body masses likely comparable to those of the microraptorines[2,10] (i.e., Galloanserae[48,49]), their hindlimb bones undergo different mechanical constraints linked to the different duration of their fledging period (i.e., phasianids have a precocial onset of flight, whereas anseriforms have a delayed one)[48]. In the appendicular elements[48], this pattern is expressed by an inverse relationship between growth rate and the functional maturity of the skeletal tissues. In particular, differing from poor-fliers (e.g., the phasianids)[48], in the fully-volant anseriforms the altricially-developing forelimb grows much faster than the precociallly-developing hindlimb bones[49]. Yet, the histological samples from the appendicular elements in the microraptorines suggest a different ontogenetically-controlled pattern. In some cases, represented by the most immature individuals sampled, there is no clear evidence of an avian-like differential regime between fore- and hindlimb[29]. In other samples based on more mature individuals, the differences between fore- and hindlimb samples might indicate an inverse pattern[15]. Yet, it is noteworthy that the radius of *Norellraptor* shows interrupted growth, circumferentially-organized osteons and osteocyte lacunae, with almost abrupt decrease of osteons within the second preserved zone and towards periphery, whereas the tibiotarsus of *Microraptor* shows uninterrupted growth, randomly-organized osteons and osteocyte lacunae, with obvious decrease of osteons towards the periphery[15]. Assuming that such "inverse" differential regime among Microraptorinae followed the same relationships between growth and function observed in living birds[48,49], this could indicate a peculiar precocially-developing forelimb pattern in the four-winged paravians, which is distinct from the growth models so far observed among modern flying avians.

https://doi.org/10.1038/s41467-026-77804-6

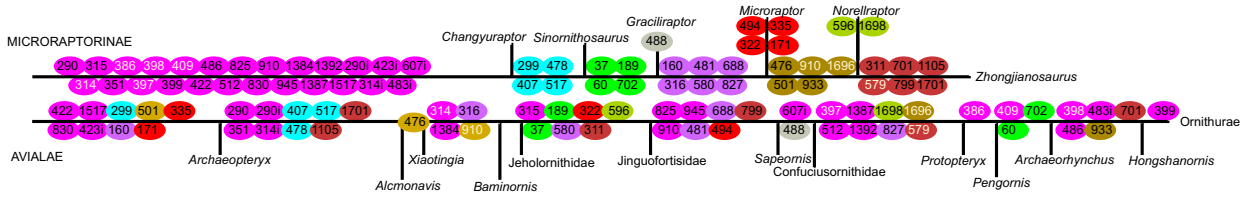

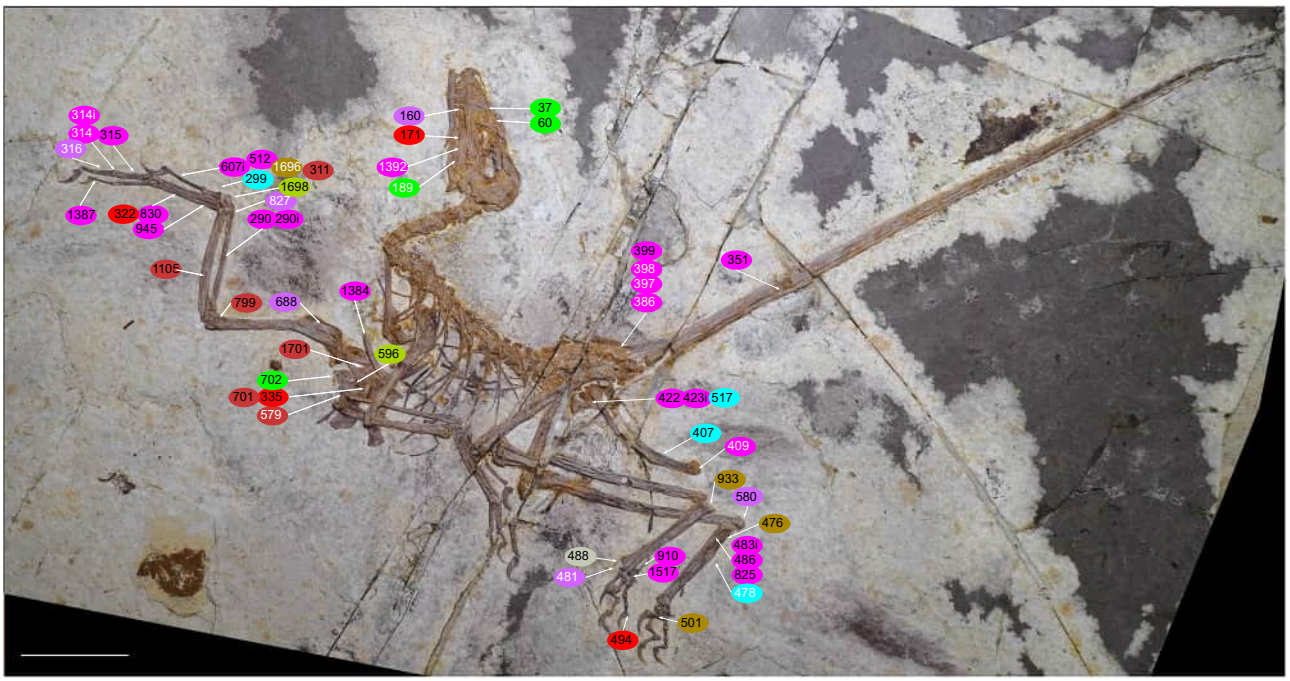

Fig. 5 | Evolutionary sequences of the derived features shared by Microraptorinae and Avialae. Numeration refers to the character states used in the phylogenetic analysis. Characters in black indicate the "0- > 1" transitions, characters in white the reversions "1- > 0". The "i" letter indicates novelties optimized as synapomorphic among the immature semaphoronts[20].

Methods

Ethical considerations and integrity of the specimen

This research complies with all relevant ethical regulations. The academic boards of both the Institute of Geology, Chinese Academy of Geological Sciences (CAGS), and the Hebei GEO University have approved the study protocol as applicable. The physical sectioning used for the histological analyses was performed in the specialized laboratory of the CAGS. The sampled material is housed at the Museum of Hebei GEO University, which can be accessed by contacting with Q.J.

The specimen was discovered by a local farmer near Lamadong Town (Jianchang County, western Liaoning, China), and donated to the museum of Hebei GEO University in 2023. The donor requested to remain anonymous. We checked the specimen's integrity and ascertained the original fossil locality. The completeness and almost undisturbed articulation of the skeletal elements, combined with the presence of microraptorine synapomorphies in all anatomical regions[1–9] unambiguously support the integrity of the specimen.

Histological analysis

A sample of a distal projection of the mid-shaft of the radius was extracted from *Norellraptor barsboldi* type specimen (130108-MHGU-F4281) to provide information about the histology of the wing zeugopodium, growth dynamics, and ontogenetic age in this dromaeosaurid (Fig. 3).

The osteohistological sample was taken from the distal end of the midshaft of the left 49 mm long radius. It was embedded in one-component resin (EXAKT Technovit 7200) and hardened in a light polymerization device (EXAKT 520). The cross-sections were processed by sub-serially cutting the trimmed block slowly with a circular diamond saw (Isomet Buehler LTD Company) and an accurate circular saw (EXAKT 300CP). The sections were ground using the EXAKT 400CS grinding system until the desired optical contrast was obtained at a thickness of 52 µm. Successive transverse views of the bone were evaluated in transmitted light, elliptically polarized light, and fluorescent light (exposure time was controlled within around 3 s) using the ZEISS AX10 microscope. Images of each slice were captured using a digital camera (ZEISS AxioCam MRc5) and further processed using CorelPHOTO Paint and CorelDRAW X5 software. Histological measurements were taken from digitized cross-sections using ImageJ.

Institutional abbreviations

DNHM, Dalian Natural History Museum, Dalian, Liaoning, China. MHGU, Museum of Hebei GEO University, Shijiazhuang, China. YFGP, Yizhou Fossil and Geology Park, Yixian, Liaoning, China.

Phylogenetic analysis

The new theropod is unambiguously referrable to Dromaeosauridae based on the combination of the ziphodont dentition, presence of caudotheca and hypertrophied falciform second toe ungual[7,27]. In order to test its particular affinities among dromaeosaurids and other bird-like dinosaurs, we included it in an updated version of the phylogenetic matrix of ref. 20 and focusing on maniraptoran coelurosaurs. The taxonomic unit based on *Norellraptor* was coded in the post-

juvenile partition[20] based on the histological analysis of 130108-MHGU-F4281. The dataset was analysed using equally weighted parsimony in TNT 1.6[50]. The data matrix and character list used for the phylogenetic analysis are deposited into the public data repository FigShare[51]. All analyses were performed setting maxtree = 50.000. We performed 1000 'Traditional search' runs using default settings, then explored the tree islands stored in the RAM during the first search round. Nodal support was calculated replicating the analysis and saving all trees up to 10 steps longer than the shortest topologies. The analysis found 50.000 shortest trees of score 8735 (Consistency Index = 0.31, Retention Index = 0.54). The topology of Microraptorinae was consistently reconstructed in all shortest trees found except for the placements of *Graciliraptor* and *Sinornithosaurus*, which were alternatively reconstructed as the closest sister taxon of the least inclusive node containing *Microraptor*, *Norellraptor* and *Zhongjianosaurus*. In order to fully resolve the topology among the microraptorines, we replicated the analysis using the Implied Weighting function of TNT 1.6[50] setting a moderate downweighting of the homoplastic character state transitions (weighting strength = 1000). All shortest trees reconstructed by the second analysis share the same topology for Microraptorinae: it broadly overlaps the result in the first analysis and places *Graciliraptor* closer to the least inclusive node containing *Microraptor*, *Norellraptor* and *Zhongjianosaurus* than *Sinornithosaurus*. We used the strict consensus of the shortest trees reconstructed by the second analysis as reference topology for character state optimization at nodes (Fig. 4).

We define Microraptorini[5] as the most inclusive clade containing *Microraptor zhaoianus*[2] but excluding *Sinornithosaurus millenii*[1]. Diagnosis: small-bodied microraptorine dromaeosaurids with promaxillary recess in rostroventral corner of antorbital fossa; caudodorsal corner of the maxillary fenestra overlapped by lip of bone; short ascending ramus of maxilla; basal constriction in posterior cheek tooth crowns; sternum with distinct anterolateral corner; scapular shaft thick without sharp borders; fenestra in deltopectoral crest; penultimate phalanx of second finger shorter than preceding phalanx; first phalanx of third finger longer than 60% of first phalanx of second finger.

Evolution of "bird-like" features among microraptorinae

We used the strict consensus of the shortest trees reconstructed by the second phylogenetic analysis (see above) as reference topology for character state optimization at nodes. We analysed the distribution of the morphological features which were convergently acquired along both microraptorine and avialan lineages (N = 57; Supplementary Table 2). In order to prevent the arbitrary oversampling of the microraptorine internodal apomorphies due to preservation artifacts, the ambiguous character state transitions were optimized using a "fast optimization" algorithm (i.e., favouring changes happening at a more inclusive internode as possible). We ranked the distribution of the character state transitions shared along the microraptorine and avialan internodes and calculated the statistical significance of their correlations in PAST 4.04[52]. The sequences along the two lineages are not significantly correlated (Spearman's rank correlation coefficient for all features = -0.08, $p = 0.50$; for the forelimb and pectoral features alone = 0.15, $p = 0.47$; Supplementary Fig. 3), a result which dismisses the hypothesis that the evolution of "bird-like" trait along Microraptorinae expressed a developmental homology shared with birds.

Nomenclatural act

The electronic version of this article in Portable Document Format (PDF) will represent a published work according to the International Commission on Zoological Nomenclature (ICZN), and hence the new names contained in the electronic version are effectively published under that Code from the electronic edition alone. This published work and the nomenclatural acts it contains have been registered in ZooBank, the online registration system for the ICZN. The ZooBank LSIDs (Life Science Identifiers) can be resolved and the associated information viewed through any standard web browser by appending the LSID to the prefix http://zoobank.org/. The LSID for this publication is: LSIDurn:lsid:zoobank.org:pub:0E152A27-070B-4B69-A2B6-524509EEE15D. The online version of this work is archived and available from the digital repository PubMed Central SCIE. The LSIDs for the new genus and species are, respectively:

LSIDurn:lsid:zoobank.org:act:3BE0E85F-F461-4EFA-A0A1-99066B888FE0

and

LSIDurn:lsid:zoobank.org:act:7B8F23DC-7118-4BFA-9D86-68EA4B07E15D.

Reporting summary

Further information on research design is available in the Nature Portfolio Reporting Summary linked to this article.

Data availability

The holotype specimen of *Norellraptor barsboldi* is housed in the Museum of Hebei GEO University, Shijiazhuang, China, and registered under the accession number 130108-MHGU-F4281. The specimen can be accessed by contacting Q.J. All morphological information and the phylogenetic data used in the study are included in the article and in the supplementary files. The phylogenetic data and the character statement list used in this study are available in the FigShare database https://doi.org/10.6084/m9.figshare.33006146.

References

1. Xu, X. et al. A dromaeosaurid dinosaur with a filamentous integument from the Yixian Formation of China. *Nature* **401**, 262–266 (1999).
2. Xu, X. et al. The smallest known non-avian theropod dinosaur. *Nature* **408**, 705–708 (2000).
3. Hwang, S. H. et al. New specimens of *Microraptor zhaoianus* (Theropoda: Dromaeosauridae) from northeastern China. *Am. Mus. Novit.* **3381**, 1–44 (2002).
4. Xu, X. et al. Four-winged dinosaurs from China. *Nature* **421**, 335–340 (2003).
5. Senter, P. et al. Systematics and evolution of Dromaeosauridae (Dinosauria, Theropoda). *Bull. Gunma Mus. Natu. Hist.* **8**, 1–20 (2004).
6. Gong, E.-P. et al. A new species of *Microraptor* from the Jehol Biota of northeastern China. *Palaeoworld* **21**, 81–91 (2012).
7. Turner, A. H. et al. A review of dromaeosaurid systematics and paravian phylogeny. *Bull. Am. Mus. Nat. Hist.* **371**, 1–206 (2012).
8. Han, G. et al. A new raptorial dinosaur with exceptionally long feathering provides insights into dromaeosaurid flight performance. *Nat. Commun.* **5**, 4382 (2014).
9. Pei, R. et al. A new specimen of *Microraptor* (Theropoda: Dromaeosauridae) from the Lower Cretaceous of western Liaoning, China. *Am. Mus. Novit.* **3821**, 1–28 (2014).
10. Pei, R. et al. Potential for powered flight neared by most close avialan relatives, but few crossed its thresholds. *Curr. Biol.* **30**, 4033–4046.e8 (2020).
11. Norell, M. A. & Xu, X. Feathered dinosaurs. *Annu. Rev. Earth Planet. Sci.* **33**, 277–299 (2005).
12. O'Connor, J. et al. Additional specimen of *Microraptor* provides unique evidence of dinosaurs preying on birds. *Proc. Natl Acad. Sci. USA* **108**, 19662–19665 (2011).
13. Li, Q.-G. et al. Reconstruction of *Microraptor* and the evolution of iridescent plumage. *Science* **335**, 1215–1219 (2012).
14. Xing, L.-D. et al. Piscivory in the feathered dinosaur *Microraptor*. *Evolution* **67**, 2441–2445 (2013).

15. Chotard, M. et al. New information on the hind limb feathering, soft tissues and skeleton of *Microraptor* (Theropoda: Dromaeosauridae). *BMC Ecol. Evol.* **25**, 37 (2025).
16. Chatterjee, S. & Templin, R. J. Biplane wing planform and flight performance of the feathered dinosaur *Microraptor gui*. *Proc. Natl Acad. Sci. USA* **104**, 1576–1580 (2007).
17. Alexander, D. E. et al. Model tests of gliding with different hindwing configurations in the four-winged dromaeosaurids *Microraptor gui*. *Proc. Natl Acad. Sci. USA* **107**, 2972–2976 (2010).
18. Dececchi, T. A. & Larsson, H. C. E. Assessing arboreal adaptations of bird antecedents: testing the ecological setting of the origin of the avian flight stroke. *PLoS ONE* **6**, e22292 (2011).
19. Dyke, G. et al. Aerodynamic performance of the feathered dinosaur *Microraptor* and the evolution of feathered flight. *Nat. Commun.* **4**, 2489 (2013).
20. Cau, A. A unified framework for predatory dinosaur macroevolution. *Boll. Soc. Paleontol. Ital.* **63**, 1–19 (2024).
21. Norell, M. A. & Makovicky, P. J. Important features of the dromaeosaur skeleton: information from a new specimen. *Am. Mus. Novit.* **3215**, 1–28 (1997).
22. Norell, M. A. & Makovicky, P. J. Important features of the dromaeosaurid skeleton II: information from newly collected specimens of *Velociraptor mongoliensis*. *Am. Mus. Novit.* **3282**, 1–45 (1999).
23. Scotland, R. W. Deep homology: a view from systematics. *BioEssays* **32**, 438–449 (2010).
24. Gould, S. J. The Structure of Evolutionary Theory (Belknap Press of Harvard Univ. Press, 2002)
25. Hall, B. K. Parallelism, deep homology, and evo-devo. *Evol. Dev.* **14**, 29–33 (2012).
26. Wedel, M. J. Evidence for bird-like air sacs in saurischian dinosaurs. *J. Exp. Zool. A* **311A**, 611–628 (2009).
27. Senter, P. et al. New dromaeosaurids (Dinosauria: Theropoda) from the Lower Cretaceous of Utah, and the evolution of the dromaeosaurid tail. *PLoS ONE* **7**, e36790 (2012).
28. Gauthier, J. Saurischian monophyly and the origin of birds. *Memoirs Cal. Acad. Sci.* **8**, 1–55 (1986).
29. Poust, A. W. et al. A new microraptorine theropod from the Jehol Biota and growth in early dromaeosaurids. *Anat. Rec.* **303**, 963–987 (2020).
30. Xu, X. & Wu, X.-C. Cranial morphology of *Sinornithosaurus millenii* Xu et al., 1999 (Dinosauria: Theropoda: Dromaeosauridae) from the Yixian Formation of Liaoning, China. *Can. J. Earth Sci.* **38**, 1739–1752 (2001).
31. Powers, M. J. et al. A new hypothesis of eudromaeosaurian evolution: CT scans assist in testing and constructing morphological characters. *J. Vertebr. Paleontol.* **41**, e2010087 (2021).
32. Xu, X. et al. A basal troodontid from the Early Cretaceous of China. *Nature* **415**, 780–784 (2002).
33. Norell, M. A. et al. A review of the Mongolian Cretaceous dinosaur *Saurornithoides* (Troodontidae: Theropoda). *Am. Mus. Novit.* **3654**, 1–63 (2009).
34. Barsbold, R. & Osmólska, H. The skull of *Velociraptor* (Theropoda) from the Late Cretaceous of Mongolia. *Acta Palaeontol. Pol.* **44**, 189–219 (1999).
35. Norell, M. A. et al. A new dromaeosaurid theropod from Ukhaa Tolgod (Ömnögov, Mongolia). *Am. Mus. Novit.* **3545**, 1–51 (2006).
36. Moutrille, L. et al. A new bird-like dinosaur from the Upper Cretaceous of Mongolia with extremely robust hands supports niche partitioning among velociraptorines. *Hist. Biol.* **37**, 1–32 (2025).
37. Xu, X. & Qin, Z.-C. A new tiny dromaeosaurid dinosaur from the Lower Cretaceous Jehol Group of western Liaoning and niche differentiation among the Jehol dromaeosaurids. *Vertebrata PalAsiatica* **55**, 129–144 (2017).
38. Brusatte, S. L. et al. The osteology of *Balaur bondoc*, an island-dwelling dromaeosaurid (Dinosauria: Theropoda) from the Late Cretaceous of Romania. *Bull. Am. Mus. Nat. Hist.* **374**, 1–100 (2013).
39. Wang, R. & Pei, R. The smallest known specimen of *Microraptor* (Dinosauria: Dromaeosauridae) from the Jiufotang Formation in northeastern China. *Hist. Biol.* **37**, 1757–1767 (2024).
40. Xu, X. & Wang, X.-L. Troodontid-like pes in the dromaeosaurid *Sinornithosaurus*. *Paleont. Soc. Korea Spec. Publ.* **4**, 179–188 (2000).
41. Cau, A. & Madzia, D. The phylogenetic affinities and morphological peculiarities of the bird-like dinosaur *Borogovia gracilicrus* from the Upper Cretaceous of Mongolia. *PeerJ* **9**, e12640 (2021).
42. Prondvai, E. et al. Intraskeletal histovariability, allometric growth patterns, and their functional implications in bird-like dinosaurs. *Sci. Rep.* **8**, 258 (2018).
43. Longrich, N. R. & Currie, P. J. A microraptorine (Dinosauria: Dromaeosauridae) from the Late Cretaceous of North America. *Proc. Natl Acad. Sci. USA* **106**, 5002–5007 (2009).
44. Motta, M. J. et al. Phylogenetic relationships of Unenlagiidae among Paraves (Dinosauria). *J. Syst. Palaeont.* **23**, 2529608 (2025).
45. Agnolín, F. L. & Novas, F. E. Unenlagiid theropods: are they members of the Dromaeosauridae (Theropoda, Maniraptora)? *An. Acad. Bras. Ciênc.* **83**, 117–162 (2011).
46. Agnolín, F. et al. Paravian phylogeny and the dinosaur-bird transition: an overview. *Frontiers in Earth Science* **6**, 252 (2019).
47. Novas, F. E. et al. Osteology of *Unenlagia comahuensis* (Theropoda, Paraves, Unenlagiidae) from the Late Cretaceous of Patagonia. *Anat. Rec.* **304**, 2741–2788 (2021).
48. Montes, L., de Margerie, E., Castanet, J., de Ricqlès, A. & Cubo, J. Relationship between bone growth rate and the thickness of calcified cartilage in the long bones of the Galloanserae (Aves). *Journal of Anatomy* **206**, 445–452 (2005).
49. Castanet, J., Grandin, A., Abourachid, A. & de Ricqlès, A. Expression of growth dynamics in the structure of the periosteal bone in the mallard *Anas platyrhynchos*. *Comptes Rendus de l'Académie des Sciences* **319**, 301–308 (1996).
50. Goloboff, P. & Morales, M. TNT version 1.6, with a graphical interface for MacOS and Linux, including new routines in parallel. *Cladistics*, (2023).
51. Wang X. et al. Phylogenetic data set of "Independent assembly of the flight apparatus in a non-avian dinosaur clade". *FigShare* https://doi.org/10.6084/m9.figshare.33006146 (2026).
52. Hammer, Ø et al. Past: Paleontological Statistics Software Package for Education and Data Analysis. *Palaeontologia Electronica* **4**, 1–9 (2001).

Acknowledgements

We thank the Willi Hennig Society for supporting the free use of the TNT software.

Author contributions

X.W. led the project, paper writing and produced the figures. Y.J. performed specimen preparation and produced the figures. A.C. conducted phylogenetic analyses, results, discussions, paper writing and produced the figures. M.K. conducted the histology analysis, results, discussions, paper writing and produced the figures. Y.L. and Y.W. performed specimen preparation. Q.J. contributed to logistics.

Funding

This work was supported by the National Natural Science Foundation of China (U2544210, 42472002) awarded to W.X., the Scientific Grant Agency VEGA of the Ministry of Education, Research, Development and Youth of the Slovak Republic (1/0075/22, 1/0259/25), and by the Slovak Research and Development Agency (APVV-21-0319, APVV-24-0161), the Scientific Grant Agency VEGA of the Ministry of Education, Research, Development and Youth of the Slovak Republic (1/0259/25), awarded to M.K.

Competing interests
The authors declare no competing interests.

Additional information
Supplementary information The online version contains supplementary material available at https://doi.org/10.1038/s41467-026-77804-6.

Correspondence and requests for materials should be addressed to Andrea Cau or Qiang Ji.

Peer review information *Nature Communications* thanks reviewers Ashley Poust, Fernando Novas and Thomas Holtz Jr for their contribution to the peer review of this work. A peer review file is available.